Talanta 269 (2024) 125379

Contents lists available at ScienceDirect

Talanta

journal homepage: www.elsevier.com/locate/talanta

Utilizing ablation volume for calibration in LA-ICP-MS mapping to address variations in ablation rates within and between matrices

Kristina Mervič [a], Johannes T. van Elteren [a,**], Marjan Bele [b], Martin Šala [a,*]

[a] Department of Analytical Chemistry, National Institute of Chemistry, Hajdrihova 19, Ljubljana, 1000, Slovenia
[b] Department of Materials Chemistry, National Institute of Chemistry, Hajdrihova 19, Ljubljana 1000, Slovenia

ARTICLE INFO

Keywords:
Laser ablation
Optical profilometry
LA-ICP-MS
Mapping
SEM-EDX

ABSTRACT

Quantification in 2D LA-ICP-MS mapping generally requires matrix-matched standards to minimize issues related to elemental fractionation. In addition, internal standardization is commonly applied to correct for instrumental drift and fluctuation, whereas also differences in ablated mass can be rectified for samples that cannot be sectioned and subjected to total ablation. However, it is crucial that the internal standard element is homogeneously distributed in the sample and that the laser light absorptivity is uniform over the surface. As in practice these requirements are often not met, this work will focus on correction of ablation rate differences within/between samples and standards by normalizing the element maps using the associated ablation volume per pixel as measured by optical profilometry. Due to the volume correction approach the element concentrations are no longer defined as mass per mass concentrations (in μg g^{-1}) but by mass per volume concentrations (in μg cm^{-3}), which can be interconverted in case matrix densities are known. The findings show that ablation volume-aided calibration yields more accurate element concentrations in 2D LA-ICP-MS maps for a decorative glass with highly varying elemental concentrations (murrina). This research presents a warning that if there are variations in ablation rates between samples and standards within and across matrices, even when their sensitivities are the same, generic LA-ICP-MS calibration protocols may not accurately depict the actual element concentrations.

1. Introduction

The development of LA cells with fast washout of aerosol particles in 2D LA-ICP-MS elemental mapping has led to major improvements in mapping speed and spatial resolution [1,2]. However, quantification of elements remains challenging due to elemental fractionation issues (non-stoichiometric effects during vaporization, transport of ablated particles, atomization, and ionization in the plasma), causing the signal measured not to be entirely representative of the composition of the sample. Furthermore, differences in mass ablated due to matrix-dependent ablation rates caused by differences in absorptivity, reflectivity, and thermal conductivity complicate the quantification process [3,4]. Several approaches have been reported to counteract these quantification problems, but so far, the most dependable solution is to matrix-match external standards and samples and the use of suitable internal standards.

Even though the availability of matrix-matched external standards is limited, especially for biological samples, they are often custom-prepared via pressing of tablets from certified biomaterial standards or from nano-particulate powders after wet-milling of refractory materials [5–7]. Internal standardization methods that correct for instrumental drift and fluctuation, but also deal with matrix effects and differences in intra-sample ablation rates, are often unpredictable and depend on the type of sample under study [8]. Approaches in use rely on i) total consumption of thin biosamples and standards [9–11], ii) application of a "film" standard on/under a biosample combined with total consumption of the assembly [12,13], iii) (in-cell or in-torch) aspiration of a standard solution during laser sampling [14–16], iv) the use of homogeneously distributed elements in the sample [17,18], and v) labelling of tissue components with a metallo-intercalator [19,20].

Total consumption approaches can correct for differences in ablation rate, but only for precisely sectioned "thin" biosamples (and standards), whereas homogeneously distributed elements or labelling approaches can also correct for ablation differences in "thick" biosamples. However, suitable elements that can act as an internal standard are rare, and for aiding the quantification process of all kinds of matrices, also inorganic

* Corresponding author.
** Corresponding author.
E-mail addresses: elteren@ki.si (J.T. van Elteren), martin.sala@ki.si (M. Šala).

https://doi.org/10.1016/j.talanta.2023.125379
Received 6 October 2023; Received in revised form 20 October 2023; Accepted 31 October 2023
Available online 3 November 2023

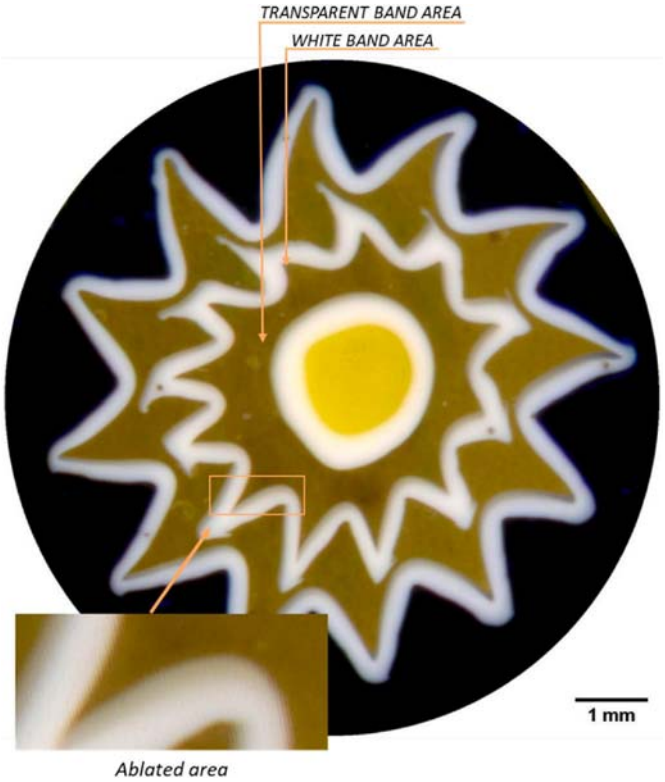

Fig. 1. Murrina used for ablation volume-aided calibration in multielement LA-ICP-MS mapping; the insert gives the actual analyzed section.

ones, a more generic approach is needed. We chose to measure the ablated volume per pixel as a means of correction for differences in ablated mass between samples and standards within and across matrices. This ablation approach yields by definition mass per volume concentrations instead of the conventional mass per mass concentrations, unless interconversion via known or measurable (local) densities of the matrices involved is possible.

As a proof-of-concept, ablation volume-aided calibration was applied for LA-ICP-MS quantification of highly variable elemental concentrations in a decorative glass (murrina). Ablation rate differences within the murrina, and between the murrina and the standards, were corrected by normalizing the element maps using the pixel-associated ablation volumes. The approach was validated using LA-ICP-MS with sum normalization calibration [21,22], as well as with scanning electron microscopy with energy dispersive X-ray spectroscopy (SEM-EDXS). To demonstrate that ablation rate variations are not so uncommon, we also analyzed a geological thin section consisting of several mineralogical phases with and without volume normalization.

2. Material and methods

2.1. Samples and standards for the volume-aided calibration approach

In the murrina production process, glass canes (long rods of glass) are formed based on stretching a compact mass of hot glass to great length, implying that it retains its radial pattern in longitudinal direction perfectly, and as such a several millimeters thick slice of the cane (=murrina) has a high depth homogeneity, making it an ideal sample for repeated mapping on the same area. A modern murrina (Murano, Italy) (Fig. 1), embedded in epoxy resin, and polished with silica carbide polishing disks (800 and 2400 grit) and diamond slurry (Diamond suspension, polycrystalline, Reflex LDP, 3 μm, Presi, France), was subjected to LA-ICP-MS multi-element mapping in line scanning mode to quantify the highly variable elemental concentrations. Glass standards used in the calibration were the NIST SRM glasses 610 and 612, having nominal concentrations of 500 and 50 μg g^{-1}, respectively, for ca. 60 elements. The proposed approach was also used to analyze a well-prepared geological thin section, which contained various mineralogical phases like garnets, cordierite, biotite, and others. This is a typical geological sample frequently analyzed by LA-ICP-MS, and will aid to demonstrate that intra-sample ablation rate variations are rather common and may need extra attention with regard to accurate quantification via volume normalization.

Table 1
Operational LA-ICP-MS settings used for multielement mapping of the murrina.

LA (Analyte G2, ARIS, and glass expansion unit)	
Wavelength (nm)	193
Laser fluence (J cm^{-2})	3.6
Repetition rate (Hz)	100
Scanning mode	Line scanning
Dosage (shots per pixel)	10
Washout time (ms)	Ca. 100
Beam size (μm)	5
Mask shape	Square
He flow rate (L min^{-1}) cup|cell	0.3|0.3
ICP-MS (Agilent 7900x)	
R_f power (W)	1500
Plasma gas flow rate (L min^{-1})	15
Auxiliary gas flow rate (L min^{-1})	0.9
Ar makeup flow rate (L min^{-1})	0.8
Data acquisition	Time-resolved
Isotopes measured	^{29}Si,^{23}Na,^{27}Al,^{39}K,^{43}Ca,^{75}As,^{137}Ba and^{208}Pb
Dwell time (ms)	10

2.2. Instrumentation and measurement protocols

Elemental mapping was performed using a laser ablation system (193 nm ArF*; Analyte G2, Teledyne Photon Machines Inc., Bozeman, MT) equipped with a standard active two-volume ablation cell (HelEx II), including the Aerosol Rapid Introduction System (ARIS, Teledyne CETAC Technologies) coupled with glass expansion unit, a so-called long pulse module having an overall aerosol particle washout time of ca. 100 ms (=FW0.01 M, full width at 1 % of the maximum). The laser ablation system was interfaced with a quadrupole ICP-MS instrument (Agilent 7900*x*, Agilent Technologies, Santa Clara, CA). The LA-ICP-MS mapping conditions for element mapping of the murrina in line scanning mode are given in Table 1. Line scanning was performed with a dosage *D* of 10, implying that signals of 10 laser shots were accumulated in the analysis time *AT* of 100 ms, requiring a repetition rate *RR* of 100 Hz ($D = RR{\cdot}AT$) [23–25]. In essence, 10 overlapping laser shots generated a square pixel equal to the beam size *BS* although the material sampled originates from a slightly larger area ($[2{\bullet}BS\text{-}BS/D] \times [BS]$). To measure the surface morphology of the murrina surface we used an optical interferometer (Zegage PRO HR, Zygo Corporation, Middlefield, CT). 3D information was recorded using a 50 × magnification lens with a lateral resolution of 0.173 μm, and a surface topography repeatability better than 3.5 nm. Data associated with the surface topography was first processed with the manufacturer's MxTM software (version 8.0.0.23), and then "sur" and "int" files were imported and converted into csv format using MatLab R2020a (MathWorks); missing data corresponding to extremely sloped areas was filled in with adjacent data using the regionfill function in MatLab. The high-resolution topography maps were resampled to match the pixel size of the LA-ICP-MS element maps, followed by registration of the different modality maps, i.e., the element and volume maps. ImageJ, OriginLab, and HDIP (Teledyne Photon Machines Inc., Bozeman, MT) software packages were used for image and data processing.

For the highest precision and accuracy, the ablation volume-aided calibration approach requires pre-knowledge about the density of the standards. To this end, we measured the density of the NIST SRM 610

Table 2
The LA-ICP-MS murrina data generated by the volume-aided calibration approach (Vol) was validated by comparing it with data obtained from LA-ICP-MS with sum normalization calibration (Sum) and SEM-EDXS. The transparent (T) and white (W) areas on the murrina were analyzed separately. The data in the table are reported as averages ±95 % confidence limits (volume concentrations converted to %m/m or μg g^{-1} concentrations), by measuring the signal and volume of multiple areas (10 × 10 pixels) for both the white and transparent parts.

Elem	Area	Vol	Sum	SEM-EDXS
Si %m/m	T	32.7 ± 0.5	31.4 ± 2.1	35.2 ± 0.2
	W	19.2 ± 0.2	20.5 ± 1.7	21.7 ± 0.1
Na	T	13.3 ± 0.5	12.7 ± 0.8	13.5 ± 0.1
%m/m	W	6.0 ± 0.1	5.9 ± 0.5	6.3 ± 0.1
Al %m/m	T	0.40 ± 0.01	0.33 ± 0.02	0.38 ± 0.04
	W	0.57 ± 0.01	0.54 ± 0.04	0.60 ± 0.03
K %m/m	T	2.3 ± 0.1	2.3 ± 0.2	2.1 ± 0.1
	W	1.7 ± 0.1	1.9 ± 0.1	1.9 ± 0.1
Ca %m/m	T	5.2 ± 0.2	5.1 ± 0.4	5.1 ± 0.1
	W	0.9 ± 0.1	0.95 ± 0.2	0.9 ± 0.2
As %m/m	T	0.±0.03	0.33 ± 0.01	0.26 ± 0.04
	W	4.9 ± 0.2	4.7 ± 0.4	4.9 ± 0.1
Pb %m/m	T	nd*	nd*	nd*
	W	31.0 ± 0.4	32 ± 2.3	31.1 ± 0.2
Ba μg g^{-1}	T	27 ± 3.3	30 ± 4.0	nd*
	W	20 ± 3.7	20 ± 2.0	nd*

*, not detectable.

and 612 standards with a gas pycnometer (1345 AccuPyc II, Micromeritics, Norcross, GA). To convert mass per volume concentrations in the murrina sample to mass per mass concentrations, the local densities need to be determined as well. As local densities cannot be determined directly, we inferred them from their local composition using a global model [26] based on concentration data obtained with SEM-EDXS (see Table 2). Calculated densities were as follows: approximately 2.49 g cm^{-3} for the transparent area and 3.20 g cm^{-3} for the white area; these data are in line with the densities of soda-lime-silica glasses and lead glass, respectively [27]. This allows us to validate the results of LA-ICP-MS volume-corrected calibration data with SEM-EDXS and LA-ICP-MS sum normalized calibration data (see Table 2).

2.3. Validation

To validate the volume-corrected calibration approach, complementary techniques were used to measure the concentrations of selected elements (see Table 1) in the white and transparent areas indicated in Fig. 1, using LA-ICP-MS with sum normalization calibration and direct SEM-EDXS analysis. The sum normalization approach is a mathematically formulated technique based on the simultaneous measurement of 54 elements and normalizing them to 100 % m/m based on their corresponding oxide concentrations [21]. Additionally, direct SEM-EDXS analysis was carried out using a FE-SEM Zeiss Supra TM 35 VP Carl Zeiss, Oberkochen, Germany) field emission scanning electron microscope equipped with an energy-dispersive X-ray spectrometer SDD EDX Ultim Max 100 (Oxford Instruments, Oxford, UK). Samples were coated with 6 nm of platinum using a precision etching coating system (PECS), model 682 (Gatan, US). The operating voltage was set to 20 kV.

3. Results and discussion

Generally, external calibration by solid sampling techniques such as LA-ICP-MS requires closely matrix-matched reference materials to account for differences in ablation rate, and the use of suitable internal standards to correct for instrumental drift and fluctuation. As matrix-matching is only possible for samples with "known" characteristics, and the fact that internal standards are usually difficult to pinpoint, we discuss here an ablation volume-aided calibration approach that corrects for temporal variations in ablated mass during elemental mapping for the best possible localized quantification of selected elements in a murrina (Fig. 1). We used a murrina because of reproducible mapping areas and the fact that concentrations can be conveniently validated via the sum normalization approach and SEM-EDXS.

3.1. Volume-corrected calibration

To perform ablation volume-corrected quantification of elements in a sample (*S*) by 2D LA-ICP-MS mapping, we not only measure the signal intensity $A_{S,i}$ (in cps), but also the volume ablated ($V_{S,i}$) (in μm^3) per pixel *i* (see Fig. 2). A number of n calibrants (*C*n) with known mass concentrations $c_{Cn,mass}$ (in μg g^{-1}) and densities D_{Cn} (in g cm^{-3}) are

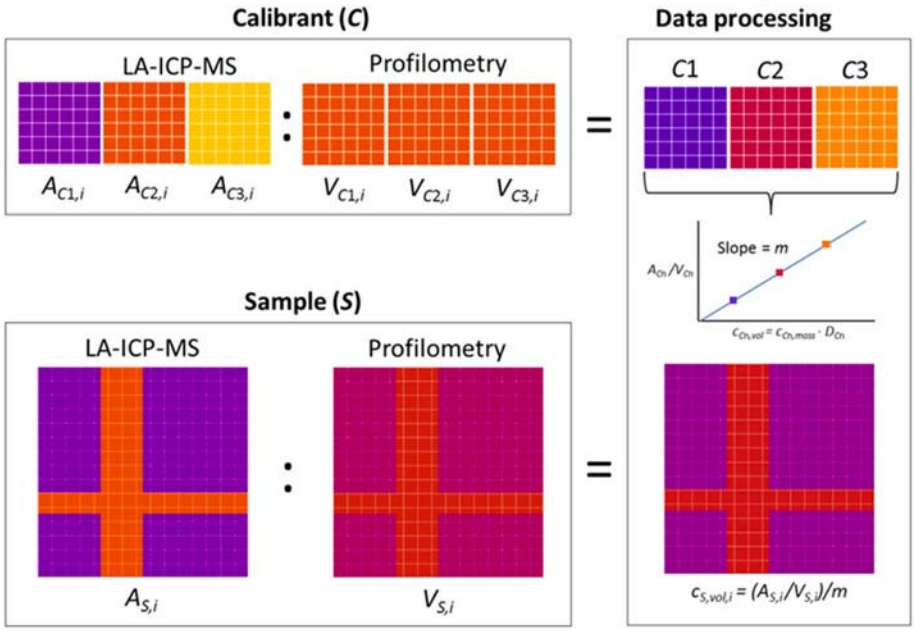

Fig. 2. Principle of the ablation volume-aided calibration approach based on LA-ICP-MS and profilometry measurements, and using calibrants (*C*1, *C*2 and *C*3) with equal densities ($D_{C1} = D_{C2} = D_{C3}$), yielding a sample map with pixels *i* showing mass per volume concentrations $C_{S,vol,i}$.

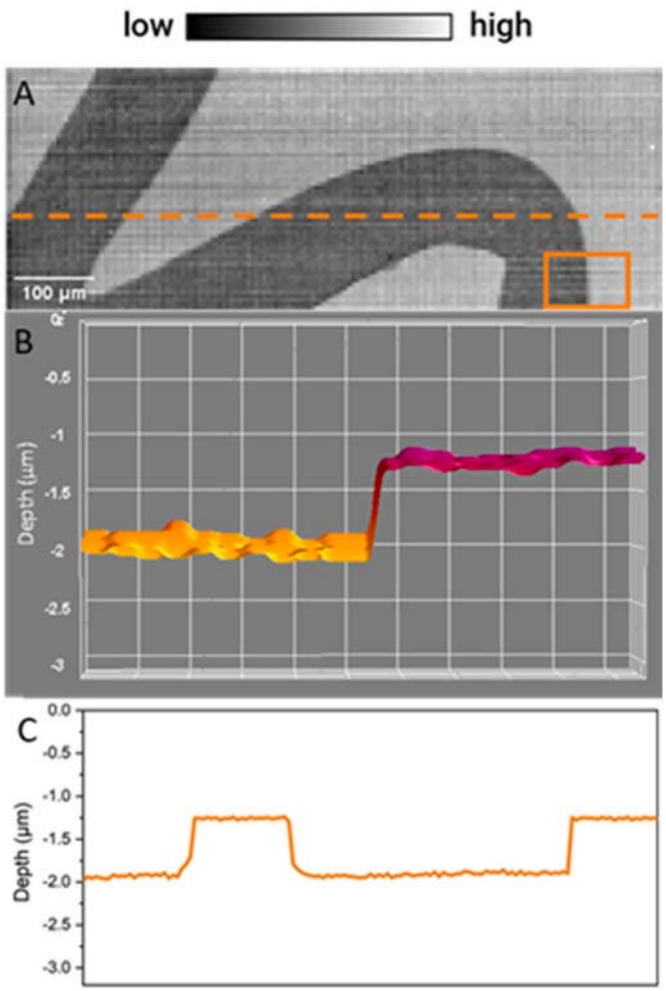

Fig. 3. Surface morphology of the ablated section of the murrina (Fig. 1, insert) measured by optical profilometry and shown as a 2D-greyscale image (A) showcasing the actual depth ablated with 10 shots with further detailing in the orange rectangle (B), and along the orange dashed line (C). The zero-levels correspond to the pristine, unablated murrina surface.

applied for external standardization; when measured similarly as the sample, the average calibrant signal intensities A_{Cn} per pixel (in cps) and the average calibrant volumes ablated V_{Cn} per pixel (in µm^3) yield a calibration graph as presented in Fig. 2. Here the average volume concentrations $c_{Cn,vol}$ of the calibrants (in µg cm^{-3}) are given by $c_{Cn,mass}{\cdot}D_{Cn}$ and the slope of the calibration graph by m (linear regression, forced through zero). The unknown volume concentrations $c_{S,vol,i}$ in pixel i of the sample (in µg cm^{-3}) are given by $(A_{S,i}/V_{S,i})/m$. Most often it is unlikely that $c_{S,vol,i}$ can be converted into $c_{S,mass,i}$ as local densities in the sample need to be known, implying that this approach generally calculates the elemental concentrations in pixels of the sample map as mass per volume concentrations. By recording pixels of calibrants and samples similarly (pixel width = scanning speed SS × acquisition time AT; pixel height = distance between line scans L), their area is uniform, and correction based on ablation volume becomes an ablation depth correction. When a sample has a flat, smooth surface prior to ablation, it suffices to merely measure the post-ablation surface, but when this is not the case both the pre- and post-ablation need to be measured to reliably construct the locally ablated volume [28].

3.2. Surface morphology

Due to the fact that the murrina has a flat and polished surface, it suffices to only measure the post-ablation surface topography. Fig. 3A shows the grayscale post-ablation topography map of an ablated section of the murrina, indicating a significant difference in ablation rate between the white and transparent areas. Fig. 3B and C detail the 3D surface depth in the area framed by the orange rectangle and the line scan depth along the orange dashed line in Fig. 3A, respectively. The ablated section has consistent ablation depths for the white (dark grey in Fig. 3A) and transparent (light grey in Fig. 3A) areas, being 1.98 and 1.25 µm, respectively. A potential reason for better ablation characteristics of the white area is that it contains a significant amount of Pb (31.1 % m/m, SEM-EDXS, Table 2), making it much softer for ablation but also denser than the transparent area which is primarily silica (75.3 % m/m, SiO_2 calculated from SEM-EDXS, Table 2). The post-ablation surface topography was also measured for NIST SRM 610 and NIST SRM 612 (data not shown), which are commonly used as matrix-matched standards for LA-ICP-MS calibration of glass samples. The ablated areas of NIST SRM 610 and NIST SRM 612 have a consistent ablation depth of 1.10 and 1.30 µm, respectively, using the same LA-ICP-MS operational settings as for the murrina sample. An image with isometric projection (Fig. S1) is added for better portrayal of the differences in laser ablation of the measured area in Fig. 3.

3.3. Volume-corrected surface quantification of major, minor and trace elements in the murrina

We selected major, minor and trace elements (Si, Na, Al, Ca, K, As, Pb and Ba) for measurement in selected locations of the murrina (Fig. 1) using optimized LA-ICP-MS conditions (Table 1) to minimize aliasing and elemental fractionation. Fig. 4A and 5A show the not volume-corrected maps (in % m/m) for Si and As obtained by direct two point calibration with the NIST SRM glasses 610 and 612. Fig. 4B and 5B show the volume-corrected maps (converted to % m/m via measured densities) for Si and As based on volume correction using the surface

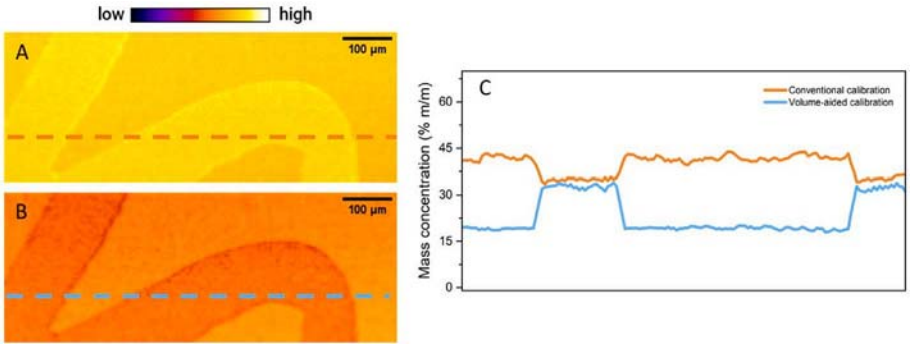

Fig. 4. LA-ICP-MS concentration map of Si in a section of the murrina (Fig. 1, insert) using conventional, not volume-corrected calibration (A) and volume-corrected calibration (B); the not-volume-corrected concentrations and corrected concentrations (in % m/m) along the dashed lines in A and B are shown in C.

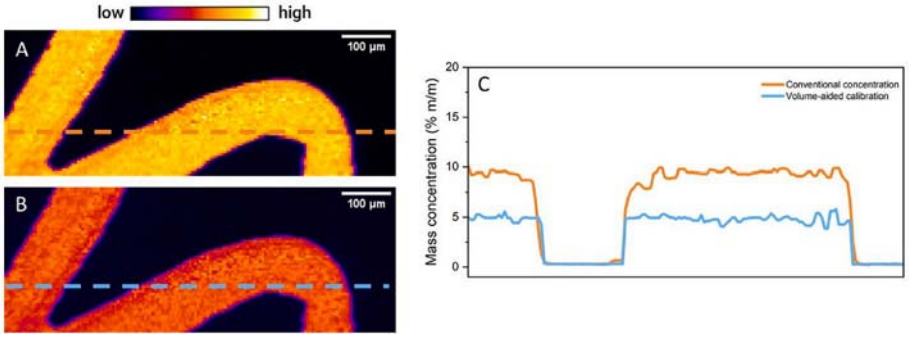

Fig. 5. LA-ICP-MS concentration map of As in a section of the murrina (Fig. 1, insert) using conventional, not volume-corrected calibration (A) and volume-corrected calibration (B); the not-volume-corrected concentrations and corrected concentrations (in % m/m) along the dashed lines in A and B are shown in C.

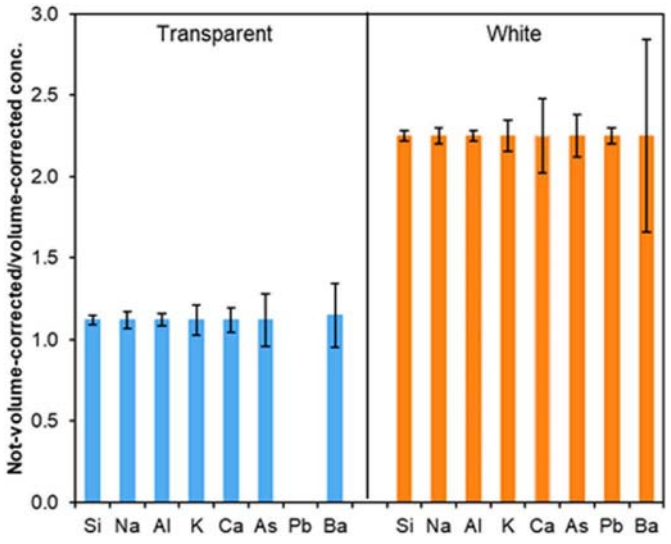

Fig. 6. Comparing the concentrations (with 95 % confidence limits) of eight elements obtained by the volume-corrected calibration approach and the not volume-corrected calibration approach in the transparent and white areas of the murrina.

topography maps in Fig. 3. Fig. 4C and 5C show the concentration profiles along the dashed lines for Si and As.

Respectively, both for the not-volume corrected data (in % m/m) and the volume-corrected data (converted to % m/m via measured densities). For the other six elements the respective maps are given in Figs. S2–S7 (Supporting information). The not volume-corrected Si map shows higher concentrations in the white area than in the transparent area, whereas for the volume-corrected Si maps the results are reversed. This suggests that the higher not volume-corrected Si concentrations in the white area are not due to an actual higher concentration, but are merely the effect of a higher mass ablated per laser shot, and thus a better representation of the actual volume concentration. This corresponds well with the high concentration of lead (31.0 % m/m, Table 2) in the white area, making the glass softer and easier to ablate. Consequently, there is less silicon on the expense of lead, therefore making the not volume-corrected maps questionable with regard to Si content. Similar to Si, in the not volume-corrected map also more As was found in the white area than in the transparent area. However, when normalized on volume, the differences between the two areas in the corrected maps become significantly smaller.

As seen from the surface morphology data (Fig. 3), different ablation rate characteristics are found for different glass areas within the murrina. This significantly affects the elemental concentrations in 2D LA-ICP-MS maps when conventional calibration is performed. We postulate that for precise quantification the volume-correction calibration approach corrects for inter- and intra-sample ablation rate differences, and yields more accurate data when the transport efficiencies and matrix sensitivities are the same.

3.4. Validation of the volume-corrected calibration approach

The volume-aided calibration approach highlighted above was validated by comparing concentrations of all eight elements in the white and transparent areas on the murrina by LA-ICP-MS with sum normalization calibration and SEM-EDXS analysis. After conversion of the volume concentration data via local densities to mass concentrations, validation of the ablation volume-corrected concentrations becomes feasible. Table 2 summarizes the results for all elements. The average concentrations obtained with the volume-aided calibration method are in good agreement with the LA-ICP-MS sum normalization and SEM-EDXS data.

However, from Fig. 6 it can be seen how the not volume-corrected data deviated significantly from the volume-corrected data, especially in the white area. The white area showcased a larger ablated volume (see Fig. 3) and higher densities compared to the transparent area and the NIST SRM glass standards, leading to higher signals due to larger amounts of ablated material entering the ICP-MS, and thus resulting in overestimation of the concentrations.

On the other hand, there is not much difference between the conventional, not volume-corrected data and the volume-corrected data for the transparent area, because the glass of the transparent area shows similar characteristics, i.e., ablation depth and density, as the NIST SRM 610 and 612 standards. This is an additional proof that exact matrix-matched standards are needed for determination of the correct concentrations by LA-ICP-MS, and confirms our hypothesis that for reliable quantification in 2D LA-ICP-MS mapping, volume-corrected elemental maps are the way forward, especially in cases where matrix-matching is problematic. Although the sum normalization approach seems the best and most convenient of all of the approaches, and might be the method of choice aiming for the most accurate results, glass is a rare example where the sum normalization can be used. For a more complex polished geological thin section sample we demonstrate (see Figs. S8 and S9, Supporting information) that considerable ablation rate differences exist within the sample, which may be dealt with by ablation volume normalization, most likely leading to improved quantification data, despite uncertainties in transport efficiencies and relative matrix sensitivities which exist for other calibration approaches as well.

4. Conclusions

Calibration has long been the Achilles' heel in LA-ICP-MS quantification as elemental fractionation, instrumental drift, and fluctuation, as well matrix-dependent ablation rates, all have to be considered in the calibration process. In this work, we have focused on investigating

(local) ablation rate differences in a decorative glass (murrina) and calibration standards upon measurement of major, minor and trace elements, and correcting for them using the ablated volume per pixel. Validation with complementary techniques has shown that conventional, not-volume calibration with supposedly appropriate standards may yield inaccurate quantification data. Furthermore, we have shown that 2D LA-ICP-MS mapping of a more complex geological sample with different phases shows ablation rate differences within the sample which can be mitigated by volume normalization of the individual pixel intensities.

This is especially relevant for "hard" (geological, metallurgical, etc.) samples which cannot be sectioned into very thin cross-sections as in the case of biosamples. Consequently, the resulting concentrations may have to be reported in m/V units (μg cm^{-3}) as intra-sample densities are mostly unknown. Further research is being conducted to demonstrate that this technique indeed delivers superior quantification data for diverse matrices. Summarizing we can say that neglecting the actual volumes ablated may result in potentially inaccurate LA-ICP-MS data when significant variations in ablation rates are found between samples and standards within and across matrices.

Credit author statement

Conceptualization: J.T.v.E. and M.Š., Investigation: K.M. and M.B. Visualization: K.M. Resources: J.T.v.E., M.Š., and M.B., Writing (review and editing): All authors.

Declaration of competing interest

The authors declare that they have no known competing financial interests or personal relationships that could have appeared to influence the work reported in this paper.

Data availability

Data will be made available on request.

Acknowledgements

The authors acknowledge the financial support from the Slovenian Research Agency ARRS (research core funding no. P1-0034 and P2-0393). K.M. thanks the Slovenian Research Agency ARRS for funding her PhD research.

Appendix A. Supplementary data

Supplementary data to this article can be found online at https://doi.org/10.1016/j.talanta.2023.125379.

References

[1] S.J.M. Van Malderen, A.J. Managh, B.L. Sharp, F. Vanhaecke, Recent developments in the design of rapid response cells for laser ablation-inductively coupled plasma-mass spectrometry and their impact on bioimaging applications, J. Anal. At. Spectrom 31 (2) (2016) 423–439, https://doi.org/10.1039/c5ja00430f.

[2] H.A.O. Wang, D. Grolimund, C. Giesen, C.N. Borca, J.R.H. Shaw-Stewart, B. Bodenmiller, D. Günther, Fast chemical imaging at high spatial resolution by laser ablation inductively coupled plasma mass spectrometry, Anal. Chem 85 (21) (2013) 10107–10116, https://doi.org/10.1021/ac400996x.

[3] S. Zhang, M. He, Z. Yin, E. Zhu, W. Hang, B. Huang, Elemental fractionation and matrix effects in laser sampling based spectrometry, J. Anal. At. Spectrom 31 (2) (2016) 358–382, https://doi.org/10.1039/C5JA00273G.

[4] I. Kroslakova, D. Günther, Elemental fractionation in laser ablation-inductively coupled plasma-mass spectrometry: evidence for mass load induced matrix effects in the ICP during ablation of a silicate glass, J. Anal. At. Spectrom 22 (1) (2007) 51–62, https://doi.org/10.1039/B606522H.

[5] A. Limbeck, P. Galler, M. Bonta, G. Bauer, W. Nischkauer, F. Vanhaecke, Recent advances in quantitative LA-ICP-MS analysis: challenges and solutions in the life sciences and environmental chemistry, Anal. Bioanal. Chem. 407 (22) (2015) 6593–6617, https://doi.org/10.1007/s00216-015-8858-0.

[6] P.A. Doble, R.G. de Vega, D.P. Bishop, D.J. Hare, D. Clases, Laser ablation-inductively coupled plasma-mass spectrometry imaging in biology, Chem. Rev (2021), https://doi.org/10.1021/acs.chemrev.0c01219.

[7] D. Garbe-Schönberg, S. Müller, Nano-particulate pressed powder tablets for LA-ICP-MS, J. Anal. At. Spectrom 29 (6) (2014) 990–1000, https://doi.org/10.1039/C4JA00007B.

[8] M. von Bremen-Kühne, H. Ahmadi, M. Sperling, U. Krämer, U. Karst, Elemental bioimaging of Zn and Cd in leaves of hyperaccumulator Arabidopsis halleri using laser ablation-inductively coupled plasma-mass spectrometry and referencing strategies, Chemosphere 305 (2022), 135267, https://doi.org/10.1016/j.chemosphere.2022.135267.

[9] M. Aramendía, L. Rello, S. Bérail, A. Donard, C. Pécheyran, M. Resano, Direct analysis of dried blood spots by femtosecond-laser ablation-inductively coupled plasma-mass spectrometry. Feasibility of split-flow laser ablation for simultaneous trace element and isotopic analysis, J. Anal. At. Spectrom 30 (1) (2015) 296–309, https://doi.org/10.1039/C4JA00313F.

[10] A. Arakawa, N. Jakubowski, G. Koellensperger, S. Theiner, A. Schweikert, S. Flemig, D. Iwahata, H. Traub, T. Hirata, Quantitative imaging of silver nanoparticles and essential elements in thin sections of fibroblast multicellular spheroids by high resolution laser ablation inductively coupled plasma time-of-flight mass spectrometry, Anal. Chem 91 (15) (2019) 10197–10203, https://doi.org/10.1021/acs.analchem.9b02239.

[11] D. Drescher, C. Giesen, H. Traub, U. Panne, J. Kneipp, N. Jakubowski, Quantitative imaging of gold and silver nanoparticles in single eukaryotic cells by laser ablation ICP-ms, Anal. Chem 84 (22) (2012) 9684–9688, https://doi.org/10.1021/ac302639c.

[12] C. Austin, D. Hare, T. Rawling, A.M. McDonagh, P. Doble, Quantification method for elemental bio-imaging by LA-ICP-MS using metal spiked PMMA films, J. Anal. At. Spectrom 25 (5) (2010) 722–725, https://doi.org/10.1039/B911316A.

[13] M. Bonta, H. Lohninger, M. Marchetti-Deschmann, A. Limbeck, Application of gold thin-films for internal standardization in LA-ICP-MS imaging experiments, Analyst 139 (6) (2014) 1521–1531, https://doi.org/10.1039/C3AN01511D.

[14] J.S. Becker, C. Pickhardt, H.-J. Dietze, Determination of trace elements in high-purity platinum by laser ablation inductively coupled plasma mass spectrometry using solution calibration, J. Anal. At. Spectrom 16 (6) (2001) 603–606, https://doi.org/10.1039/B008519G.

[15] V.L. Dressler, D. Pozebon, M.F. Mesko, A. Matusch, U. Kumtabtim, B. Wu, J. Sabine Becker, Biomonitoring of essential and toxic metals in single hair using on-line solution-based calibration in laser ablation inductively coupled plasma mass spectrometry, Talanta 82 (5) (2010) 1770–1777, https://doi.org/10.1016/j.talanta.2010.07.065.

[16] S.F. Boulyga, C. Pickhardt, J.S. Becker, New approach of solution-based calibration in laser ablation inductively coupled plasma mass spectrometry of trace elements in metals and reduction of fractionation effects, At. Spectrosc 25 (2004) 53–63, https://doi.org/10.46770/AS.2004.02.001.

[17] A. Kindness, C.N. Sekaran, J.r. Feldmann, Two-Dimensional mapping of copper and zinc in liver sections by laser ablation–inductively coupled plasma mass spectrometry, Clin. Chem 49 (11) (2003) 1916–1923, https://doi.org/10.1373/clinchem.2003.022046.

[18] J. Koelmel, D. Amarasiriwardena, Imaging of metal bioaccumulation in Hay-scented fern (Dennstaedtia punctilobula) rhizomes growing on contaminated soils by laser ablation ICP-MS, Environ. Pollut. 168 (2012) 62–70, https://doi.org/10.1016/j.envpol.2012.03.035.

[19] D.A. Frick, C. Giesen, T. Hemmerle, B. Bodenmiller, D. Günther, An internal standardisation strategy for quantitative immunoassay tissue imaging using laser ablation inductively coupled plasma mass spectrometry, J. Anal. At. Spectrom 30 (1) (2015) 254–259, https://doi.org/10.1039/C4JA00293H.

[20] S.J.M. Van Malderen, T. Van Acker, B. Laforce, M. De Bruyne, R. de Rycke, T. Asaoka, L. Vincze, F. Vanhaecke, Three-dimensional reconstruction of the distribution of elemental tags in single cells using laser ablation ICP-mass spectrometry via registration approaches, Anal. Bioanal. Chem. 411 (19) (2019) 4849–4859, https://doi.org/10.1007/s00216-019-01677-6.

[21] J.T. van Elteren, N.H. Tennent, V.S. Šelih, Multi-element quantification of ancient/historic glasses by laser ablation inductively coupled plasma mass spectrometry using sum normalization calibration, Anal. Chim. Acta 644 (1–2) (2009) 1–9, https://doi.org/10.1016/j.aca.2009.04.025.

[22] Y. Liu, Z. Hu, S. Gao, D. Günther, J. Xu, C. Gao, H. Chen, In situ analysis of major and trace elements of anhydrous minerals by LA-ICP-MS without applying an internal standard, Chem. Geol. 257 (1–2) (2008) 34–43, https://doi.org/10.1016/j.chemgeo.2008.08.004.

[23] J.T. van Elteren, V.S. Šelih, M. Šala, Insights into the selection of 2D LA-ICP-MS (multi)elemental mapping conditions, J. Anal. At. Spectrom 34 (9) (2019) 1919–1931, https://doi.org/10.1039/c9ja00166b.

[24] M. Šala, V.S. Šelih, C.C. Stremtan, T. Tămaș, J.T. van Elteren, Implications of laser shot dosage on image quality in LA-ICP-QMS imaging, J. Anal. At. Spectrom 36 (1) (2021) 75–79, https://doi.org/10.1039/d0ja00381f.

[25] J.T. van Elteren, V.S. Šelih, M. Šala, S.J.M. Van Malderen, F. Vanhaecke, Imaging artifacts in continuous scanning 2D LA-ICPMS imaging due to nonsynchronization issues, Anal. Chem 90 (4) (2018) 2896–2901, https://doi.org/10.1021/acs.analchem.7b05134.

[26] A. Fluegel, Global model for calculating room-temperature glass density from the composition, J. Anal. At. Spectrom 90 (8) (2007) 2622–2625, https://doi.org/10.1111/j.1551-2916.2007.01751.x.

[27] D.C. Giancoli, Physics: principles with applications, Pearson (2014).

[28] J.T. van Elteren, D. Metarapi, K. Mervič, M. Šala, Exploring the benefits of ablation grid adaptation in 2D/3D laser ablation inductively coupled plasma mass

spectrometry mapping through geometrical modeling, Anal. Chem (2023), https://doi.org/10.1021/acs.analchem.3c00774.